RFID-based Driving Fatigue Detection

[†]Chao Yang, [‡]Xuyu Wang, and [†]Shiwen Mao [†]Department of Electrical and Computer Engineering, Auburn University, Auburn, AL 36849-5201, USA [‡]Department of Computer Science, California State University, Sacramento, CA 95819-6021, USA Email: czy0017@auburn.edu, xuyu.wang@csus.edu, smao@ieee.org

Abstract—With the growth of the number of vehicles and car accidents, driving safety is becoming increasingly important. There is a compelling need for an effective, low-cost driving fatigue detection system. In this paper, we propose an RFID based system, termed NodTrack, to detect the nodding movements of drivers, which is a key indicator of fatigue and one of the most dangerous motions during drowsy driving. The NodTrack system utilizes the phase difference between two RFID tags mounted on the back of a hat worn by the driver, to extract nodding features. We propose an effective technique to mitigate the cumulative error caused by frequency hopping in most FCC-compliant RFID systems, as well as a long short-term memory (LSTM) autoencoder model to learn the nodding features from calibrated data. The highly accurate detection performance of the proposed system is validated by our experimental study.

I. INTRODUCTION

Driving fatigue is now considered as a primary cause of traffic accidents. It is reported by the National Highway Traffic Safety Administration (NHTSA) that, over 72,000 reported crashes involved drowsy driving from 2009 to 2013, and 16.5% of fatal crashes are caused by driving fatigue [1]. People's lives are at high risk in such accidents caused by drowsy driving. According to the NHTSA report, 795 lives have been lost due to drowsy driving in 2017 [2]. The number can be greatly reduced if an effective driving fatigue alarm system is available. However, most drowsy driving events are hard to detect with the existing technologies in commodity vesicles. Thus, there is a compelling demand for an effective driving fatigue detection system, which can accurately detect driving fatigue and alarm drivers to avoid accidents.

Driving fatigue detection is a popular topic in the research community for quite some time, and different types of signals have been utilized to address this issue, such as electroencephalogram (EEG), video, WiFi, and ultra sound. EEG signal can achieve high fatigue detection accuracy [3], but the driver is required to wear multiple special devices, which is not suitable for long time driving. In contrast, computer vision based techniques only need to collect eyelid movements using a camera [4]. Although the required hardware, i.e., a camera, is cheaper than that in EEG based techniques, the system performance is heavily affected when the driver wears sunglasses and may require sufficient lighting in the car. Several devicefree approaches have also been proposed. For example, WiFi signals can be used to detect driving fatigue by extracting driver's movements and breathing rate from channel state information (CSI) [5]. However, the WiFi signal is sensitive to the interference from surroundings, such as the movements of passengers and objects outside the vehicle. Features of drowsy driving can be detected by acoustic-based technique as well [6], but mitigating the influence of interference from passengers is still a big challenge.

RFID sensing has drawn increasing attention recently, which has been used for drone navigation [7], [8], gesture recognition [9], [10], breathing monitoring [11], [12], temperature sensing [13], and localization [14]. Since RFID is a near-field communication technique, interference from passengers or surroundings of the vehicle can hardly affect the sensing performance. Furthermore, the cost of the system is lower than other existing approaches. Therefore, RFID is highly suited for driving fatigue detection within the in-car environment. However, there are still many challenges to make RFID based driving fatigue detection work, such as the discontinuity in collected channel state data caused by frequency hopping, and effective feature extraction for driving fatigue detection.

In this paper, we propose an RFID based driving fatigue detection system, termed NodTrack, to fully exploit RFID based sensing and advanced machine learning for highly accurate drowsy detection. First, we introduce the model for the collected phase in a commercial RFID system and the effect of cumulative error on sampled phase data, which is caused by the frequency hopping offset in FCC-compliant RFID systems. Then, we present the design of the proposed NodTack system, elaborating on its key components such as data sensing, movement feature extraction, offline training, and online drowsy detection. Specifically, to effectively extract the nodding features from collected data, we calculate the phase difference between two tags attached to a hat worn by the driver with a specific tag deployment. To minimize the influence of cumulative error on feature extraction, we filter and differentiate the calibrated phase difference before using it to train the machine learning model. Our analysis also clearly explains why such a filtering and differentiation operation works well. Since the normal driving data is hard to obtain and label, an unsupervised LSTM autoencoder is leveraged for offline training and online driving fatigue detection. Finally, nodding is detected by measuring the Mean Absolute Error (MAE) between the input data and the output data reconstructed by the well-trained LSTM autoencoder model.

The main contributions of this paper are summarized below.

- To the best of our knowledge, this is the first work to employ commercial RFID tags for driving fatigue detection for in-car environments.
- We propose a specific tag deployment and signal processing algorithms to effectively distinguish the nodding features from other types of head movements. We also

propose a new method to estimate the phase difference between two tags in real-time RFID sensing systems.

- We analyze the influence of the cumulative error caused by the frequency hopping offset in FCC-compliant UHF RFID systems, and propose a method to effectively mitigate the impact of the cumulative error with a filtering and differentiating operation.
- Driving fatigue is detected with an unsupervised model, which does not require labeled training data that are hard and costly to obtain.
- The NodTrack system is implemented with commercial RFID tags and a reader, and evaluated by experiments, where its high detection accuracy is validated.

In the reminder of this paper, the preliminaries are introduced in Section II. We present details of the NodTrack system design in Section III and evaluate its performance in Section IV. Section V summaries this paper.

II. PRELIMINARIES

A. Measured Phase at an RFID reader

To distinguish different head movements, we need to detect and analyze the variation of distance between the reader and the target tags attached to the driver's hat. Such changes can be represented by the phase values collected by the RFID reader. According to the low level reader protocol, the reader can provide low level data, such as radio frequency (RF) phase, Received Signal Strength Indicator (RSSI), and Doppler Shift, for received tag responses [15]. The received phase value can be written as [12]

$$\varphi = \operatorname{mod}\left(2\pi(2L)/\lambda + \varphi_R + \varphi_T + \varphi_{tag}, 2\pi\right), \tag{1}$$

where L is the distance between the reader and the target tag, λ is the wavelength of the signal, φ_R and φ_T represent the phase offsets caused by the receiver and transmitter, respectively, and φ_{tag} is the phase shift caused by the refection circuit of the target tag. Since λ , φ_R , φ_T , and φ_{tag} are constant when the the reader operates at a given frequency, the change in the tag-to-reader distance L can be estimated by the change in the collected phase value φ .

B. Frequency Hopping Offset and Cumulative Error

However, according to FCC regulations, Ultra High Frequency (UHF) RFID readers should adopt frequency hopping to benefit from the maximum reader transmitted power allowances, over 50 different channels from 902 MHz to 928 MHz during tag scanning. Since the values of λ , φ_R , φ_T , and φ_{tag} in (1) vary with different frequencies, the measured phase is severely affected by both the tag-to-reader distance and the current occupied channel.

Define the measured phase for channel k as:

$$\varphi(f_k, L) = \operatorname{mod}(4\pi L f_k / c + \varphi_k, 2\pi), \qquad (2)$$

where c is the speed of light, f_k is carrier frequency of channel k, and φ_k represents initial phase offset on channel k due to φ_R , φ_T , and φ_{tag} .

Fig. 1 shows the raw phase data collected by the reader. It can be seen that the frequency hopping offset causes

considerable discontinuity in the measured phase data, and the variation of L is hard to observe from the raw phase data. To address this issue, some solutions have been proposed in recently works. For example, the Tagyro system requires a calibration process of 10 seconds to estimate the initial phase offset for each channel, and then subtract it from the measured phase data [16]. This method is not suitable for RFID systems in a driving environment, because the movements of drivers and passengers during the calibration process could affect the accuracy. In our recent work Autotag [12], we propose a realtime method to mitigate the frequency hopping effect [12]. Rather than estimating the initial phases on all channels, the Autotag system focuses on removing the phase offset between two adjacent channels. Accordingly, the phase data measured from the current channel is transformed to that on the previous channel, thus making FCC-compliant RFID systems suitable for realtime sensing applications.

The method in [12] can mitigate most of the frequency hopping offset. However, there is still some residual error remains, which will cumulate to become larger and larger as the reader hops among more and more channels. For respiration rate monitoring considered in [12], such cumulated error can be effectively removed with a detrending process. However, for driving fatigue detection considered in this paper, the information of head movements is also embedded in the low frequency components, which will be lost if the detrending process is applied. In Fig. 2, we plot the phase data collected from the tag attached on a still object and calibrated using the technique in [12]. It can be seen that although the object is not moving, the calibrated phase still keeps on changing. This is because the residual error in estimating the initial phase offset for each channel happens every 0.2s (when the reader hops to a new channel), and the error starts to accumulate over time. Since head movements will introduce a similar effect on calibrated phase, extracting movement features from the calibrated phase signal becomes a big challenge.

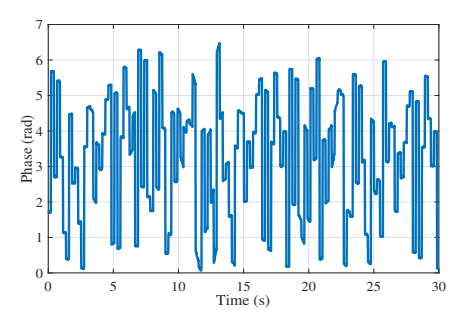
III. THE NODTRACK SYSTEM DESIGN

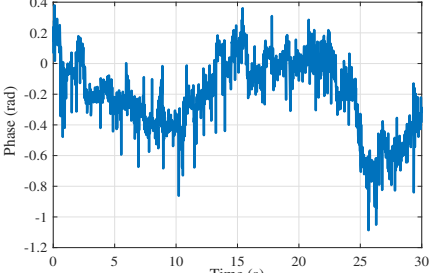
A. System Overview

We term our proposed system *NodTrack*, whose architecture is shown in Fig. 4. The system is composed of four main modules, including data sensing, movement feature extraction, offline training, and online drowsy detection. First, the RFID reader is used to collect low level data from two tags attached to the driver's hat in the data sensing module. Next, the features of head movement will be extracted from the collected data in the feature extraction module, which includes phase difference estimation, channel hopping offset mitigation, lowpass filtering, and derivative calculation. Then we train the LSTM variational autoencoder model using calibrated data. Finally, online nodding detection is executed with the well-trained model, by calculating the divergence between the input signal and the reconstructed signal. The details of the proposed system will be discussed in the remainder of this section.

B. Nodding Features Extraction

In many machine learning based systems, offline training requires a large amount of featured data. However, it's a big





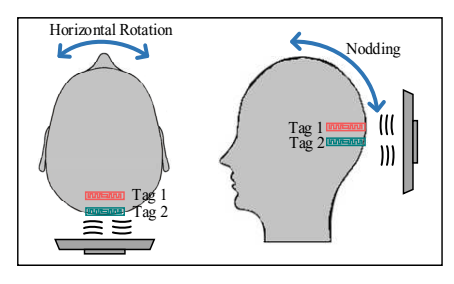


Fig. 1. Raw phase data collected by the RFID Fig. 2. An example of cumulative error in of head (e.g., on a hat). reader.

challenge to learn the features of normal driving based on head movement, because drivers may randomly rotate their head to left or right to check side-view mirrors or traffic in different lanes, which makes the head movement during normal driving unpredictable. In contrast, nodding is a typical symptom of driving fatigue, which can be labeled simply from collected data. Therefore, we extract the features of nodding from collected data for training our model. There are still some challenges remaining. First, drivers may change their posture or move their head forward or backward during driving, which makes the head movement to include both 3-D rotations and position shifts. It is difficult to separate the head shifting signal from the collected signal, because phase value is affected by both types of movements. Second, the nodding features are hard to distinguish from head rotation. This is because both movements can be considered as a round-trip rotation of the head, which makes the corresponding phase variations very similar. Finally, as discussed in Section II, the cumulative error caused by the channel hopping offset is still a big problem. In the following subsections, we address all these challenges and show how to effectively extract the nodding features.

1) Phase Difference Calculation: To mitigate the influence of driver's body movement on collected data, we calculate the phase difference between two tags and use it in NodTrack. Since the driver is buckled up, the body movement is usually constrained, and thus typical head movements consist of shifting, rotation, and nodding. Although a head shift affects the phase value of each tag, the influence on the phase difference between the two tags could be negligible [17]. This is because the head shift generates the same alteration of tag-to-reader

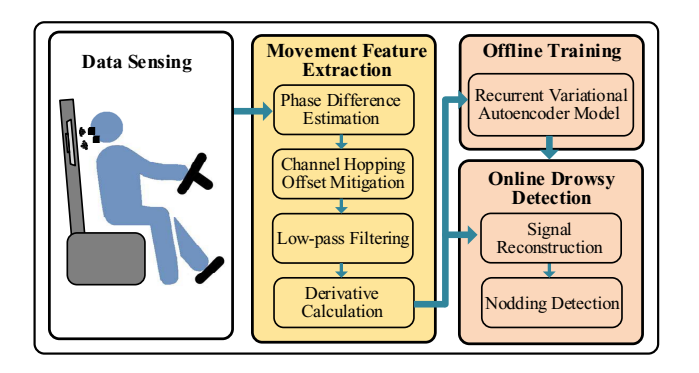


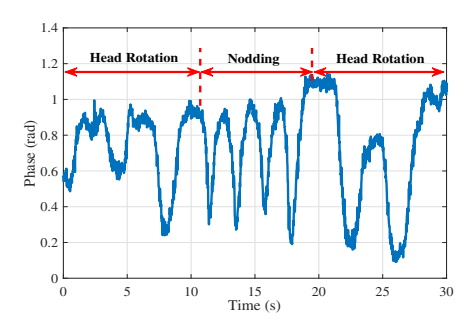
Fig. 4. Architecture of the proposed NodTrack system.

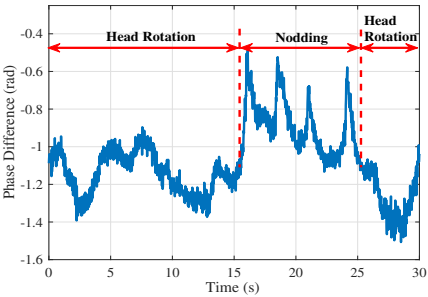
distance for both tags, resulting in the same phase shift and a negligible phase difference. In contrast, both nodding and head rotation could cause different alterations in the tag-to-reader distances of the tags, resulting in a large phase difference. Thus, phase difference is more suited for extracting nodding features than phase values collected from a single tag.

Unfortunately, following the RFID anti-collision protocol, only one RFID tag can send its EPC to the reader in every time slot, which means the phase values are sampled sequentially. Therefore, we cannot obtain the phase values from both tags at the same time to calculate the phase difference. To address this issue, we propose a new method to estimate the phase difference on each individual channel. First, we collect the phase values sampled on the same channel from the two tags, denoted by sets P_{tag1} and P_{tag2} , respectively, together with time stamps. Second, for each phase sample in P_{tag1} , we search for the Tag 2 phase sample that has the nearest time stamp. Finally, a new phase sample sequence \hat{P}_{tag2} will be selected from P_{tag2} , and phase difference will be calculated between the corresponding samples in \hat{P}_{tag2} and P_{tag1} .

2) Tag Deployment and Data Collection: After the influence from head shift is successfully mitigated, we next distinguish nodding from head rotation. Fig. 5 shows the calibrated phase data from a single tag after frequency hopping offset mitigation. The data is sampled when the driver nods and looks around (i.e., head rotation) repeatedly, as marked in the figure. However, it is hard to differentiate nodding from head rotation based on the calibrated phase data, because both movements generate sharp peaks in phase values. For the purpose of extracting unique nodding features, we adopt a simple solution with a specific tag deployment. As shown in Fig. 3, the tags are attached to the back side of the head horizontally (i.e., on a hat). When the driver looks around to check traffic, the head movement can be approximately considered as a horizontal rotation. Such a head rotation causes the same change in the tag-to-reader distance for both tags, so that the change in phase difference is negligible. In contrast, during nodding, one tag moves closer to the reader while the other tag moves away from the reader. Hence the phase difference between the tags will increase immediately.

Fig. 6 shows the calibrated phase difference between two tags horizontally placed on the back side of the head. The data is sampled when the driver is nodding and rotating the head repeatedly, as marked in the figure. We find that the





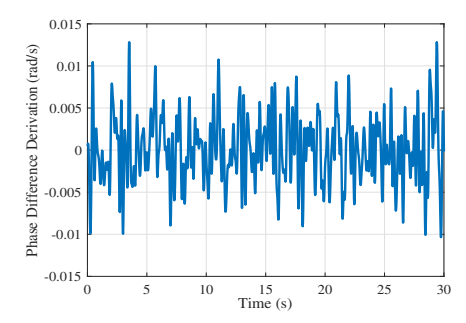


Fig. 5. Measured phase data from a single RFID Fig. 6. Calibrated phase difference between two tag.

horizontally attached tags.

Fig. 7. Derivative of raw phase difference.

data sampled during nodding is sufficiently different from that sampled in the rotation period; head rotation does not generate sharp peaks on calibrated phase difference. Thus nodding features can be effectively extracted from the phase difference between the two tags deployed as shown in Fig. 3.

3) Mitigating the Cumulative Error: To further improve the feature extraction performance, the cumulative error due to frequency hopping should be addressed, because the calibrated phase difference may be significantly distorted after a long period of driving. To address this issue, we first provide an analysis of the cumulative error. According to (1), the raw collected phase difference can be simply expressed as:

$$\Delta\varphi(L_a, L_b) = \operatorname{mod}(4\pi(L_a - L_b)f_k/c + \Delta\varphi_k, 2\pi), \quad (3)$$

where L_a and L_b are the tag-to-reader distance from Tag 1 and Tag 2, respectively, $\Delta \varphi_k$ is the initial phase offset difference between the two tags. Note that our analysis is mainly focused on the influence of the initial phase offset. So we neglect the multipath effect and mutual coupling between the two tags, and assume the phase difference is only affected by the tagto-reader distances and frequency hopping.

Since we calibrate the data by mapping all phase difference data on the current channel to the previous channel [12], all the calibrated data can be considered as sampled on the first channel. However, the estimation error of the initial phase offset accumulates each time we convert data from a new channel to the previous channel. Thus the calibrated phase difference can be written as:

$$\begin{split} &\Delta\varphi(L_a,L_b)\\ &= \mathrm{mod}\left(4\pi(L_a-L_b)f_1/c + \Delta\varphi_1 + \sum_i \delta_i, 2\pi\right), \end{split} \tag{4}$$

where f_1 and $\Delta \varphi_1$ are the frequency and initial phase offset difference on the first channel, respectively, δ_i represents the estimation error generated for the ith frequency hopping. In (4), $\sum_i \delta_i$ is hard to be eliminated from the collected data, because we do not know the accurate values of L_a , L_b , and $\Delta \varphi_1$. However, if we differentiate both sides of (4), we can stop the error accumulation over time. Suppose channel hopping starts from channel 1. When the system hops to channel k, it collects n_k samples (i.e., calibrated phase difference data) on the channel. The derivative of the channel k samples at time

 $n, n \in \{1, 3, ..., n_k\}$, can be derived as:

$$\Delta \varphi'_n(L_a, L_b) \qquad (5)$$

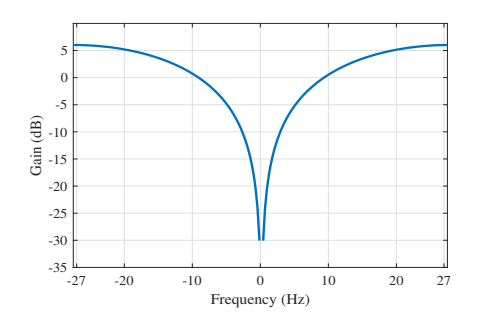
$$= \begin{cases}
\frac{4\pi f_1}{c} (L'_a - L'_b) + \delta'_{k-1}, & n = 1 \\
\frac{4\pi f_1}{c} (L'_a - L'_b), & n = 2, 3, ..., n_k,
\end{cases}$$

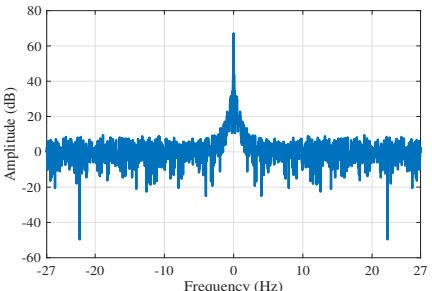
where L_a' and L_b' are the differences of tag-to-reader distances of Tag 1 and Tag 2, respectively, and δ_k' is the derivative of δ_k with $\delta_0' = 0$. We can see from (5) that although estimation error still remains in the derivative of the first sample when the system hops to a new channel, it has been removed from the derivatives of the remaining samples on the channel.

However, the derivative of phase difference cannot be directly used to extract nodding features because of the large noise. In Fig. 7, we plot the derivative of the signal plotted in Fig. 6. We find that the nodding features, which are quite obvious in Fig. 6, however, are completely overwhelmed by the white noise. This is because the differentiation operation can be considered as a high pass filter applied to the original signal. For convenience, we first assume that all phase differences are sampled at the same sample rate of 55Hz (as tested in our experiments). Then the differentiation operation can be transformed into a convolution between the input signal and a vector [F, -F], where F is the sampling frequency. If we apply DFT on [F, -F], we can obtain the frequency response as shown in Fig. 8. The figure shows that differentiation leads to extremely large gains at high frequencies, while significantly suppressing the signal at low frequencies. The frequency domain response of calibrated phase difference signal is plotted in Fig. 9, which clearly shows that the head movement features mainly exist from 0Hz to 5Hz. The Fig. 7 results are actually caused by the greatly amplified high frequency noise and greatly suppressed low frequency nodding features. To mitigate such negative impact, we apply a low pass filter with a 5Hz cutoff frequency to the calibrated phase difference before the differentiation operation. The final results after filtering and differentiation are plotted in Fig. 10. There is no cumulative error remaining in the signal anymore, and the nodding features can be clearly distinguished from other types of head movements.

C. Driving Fatigue Detection

To learn the nodding features from sampled data during driving, we leverage an unsupervised LSTM variational autoencoder. After the model is well trained, the input signal





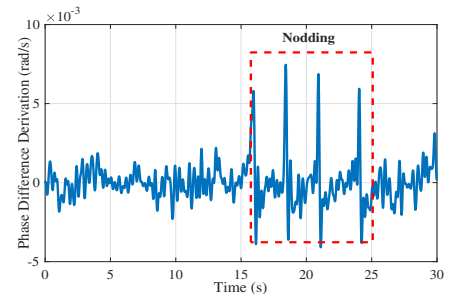


Fig. 8. The differentiation effect.

Fig. 9. Phase difference in the frequency domain. Fig. 10. Derivative of the filtered phase difference.

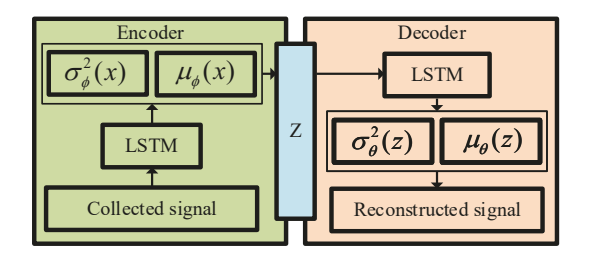


Fig. 11. The recurrent variational autoencoder for driving fatigue detection.

can be well reconstructed by the autoencoder if the signal is sampled during nodding. Otherwise, the reconstructed signal will contain high distortion. Thus, we can detect nodding by calculating the divergence between the input signal and the reconstructed signal. The details of the training model and divergence calculation are introduced in the following.

1) The Learning Model and Training: The learning model adopted for offline training is composed of an LSTM network and an autoencoder [12], which is an unsupervised learning model as shown in Fig. 11.

Consider that all the data are sampled as a time sequence, and nodding causes an obvious change of calibrated phase difference, as shown in Fig. 10. LSTM is an effective tool for capturing the nodding features, because LSTM can better learn the long-range dependency in data than traditional recurrent neural networks. The mean vector and the variance vector are estimated by two liner modules from the output of LSTM, which are employed to calculate the latent vector z in the autoencoder, as $z = \mu_{\phi}(x) + \sigma_{\phi}(x) \odot \epsilon$, where $\mu_{\phi}(x)$ is the mean vector, $\sigma_{\phi}^2(x)$ is the variance vector, ϵ represents a Gaussian noise, and \odot represents the element-wise product operation. Based on the latent vector, the variance vector $\sigma_{\phi}^2(z)$ and mean vector $\mu_{\phi}(z)$ for the reconstructed signal can be decoded from the LSTM network. Eventually, the input signal can be reconstructed as the output of the decoder.

2) Online Drowsy Detection: After offline training, the newly collected signal in realtime can be reconstructed by the network. Since our LSTM-autoencoder model has been trained by nodding features, the new signals sampled during nodding can be better reconstructed than the signals sampled during other types of head movements (and when there are no head movements). Thus, we can detect if the driver is nodding or not, by calculating the divergence between the input signal and the reconstructed signal.

In the NodTrack system, we adopt a sliding window with 2s

size to extract the input signal from calibrated phase difference to guarantee that all nodding movement can be captured in the window. The divergence is calculated in the form of Mean Absolute Error (MAE), which can be expressed as: MAE = $\frac{1}{n} \sum_{i=1}^{n} |y_i - y_i^r|$, where n is the total number of samples in the sliding window, y_i is the *i*th sample of the input signal, and y_i^r is the *i*th sample of the reconstructed signal. Then we group the MAEs from nodding and normal driving respectively, and plot all the errors in the form of cumulative distribution function in Fig. 12. The figure shows that 91.26% MAEs of the nodding signal is lower than the minimum error of the reconstructed normal driving signal, which is 0.21. Thus, we conclude that nodding movement can be effectively distinguished by MAE from other head movements. Finally we set the threshold of MAE as 0.23 for the proposed drowsy detection system.

IV. EXPERIMENTAL STUDY

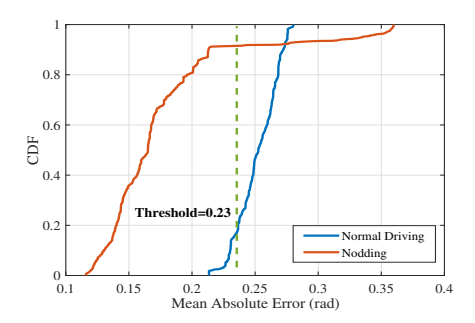
A. Test Configuration

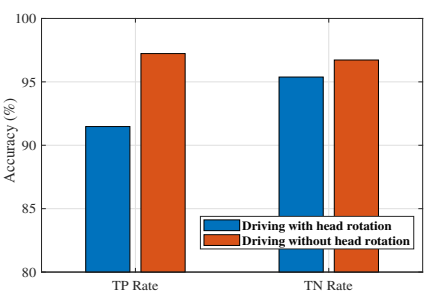
To evaluate the proposed drowsy detection system, we attach 2 passive RFID tags ALE-9470 on the back side of a hat worn by the driver. The tags are scanned by an off-the-shelf RFID reader Impinj R420, which is equipped with a polarized antenna S9028PCR. Low level data, such as RFphase, RSSI, and timestamps are provided by the RFID reader using the Low Level Reader Protocol (LLRP). The reader hops among 50 channels from 902MHz to 928MHz following FCC regulations. All sampled data will be processed in an MSI laptop computer with a Navidia GTX 1080 GPU and Intel Core i7-6820HK CPU.

The experiments are conducted in a $8.8 \,\mathrm{m} \times 4.5 \,\mathrm{m}$ laboratory, and three volunteers are involved in the experiments. The volunteers are required to wear a hat with two RFID tags attached, and emulate driving actions on a chair. During driving emulation, the volunteers can nod, rotate their head, and move their body naturally, while the reader continuously interrogates the tags on the hat. Then, all collected data are transmitted to the laptop for calibration and nodding detection.

B. Results and Discussions

The experimental results of our drowsy detection system are presented in Fig. 13. The figure shows the True Positive (TP) and True Negative (TR) rates in two different scenarios, where TP rate means the accuracy of nodding detection, and TN rate is the accuracy of normal driving recognition. For the





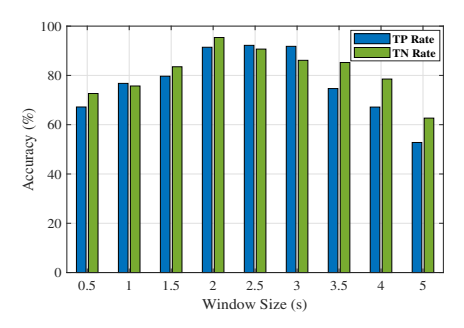


Fig. 12. CDFs of the mean absolute errors for Fig. 13. Detection accuracy in two scenarios: TP Fig. 14. Impact of the window size used for normal driving and nodding.

first scenario, the volunteers are asked to never rotate their head but only nod during the test. For the other scenario, the volunteers can move their head and body casually. The results show that our system can achieve a 97.23% TP rate and a 96.72% TN rate when no other head movements are present. The achieved TP rate and TN rate are 91.48% and 95.38%, respectively, even though the drivers rotate or shift their heads during the experiment. The high detection accuracy in different scenarios proves that our system can effectively mitigate the influence of head rotation and shifting during driving.

Fig. 14 shows the impact of the sliding window size used in offline training. The figure presents the TP rate and TN rate when the training dataset has different sliding window size from 0.5s to 5s. When the window size is smaller than 1.5s, the TP rate is lower than 79.67% and the TN rate is lower than 83.51%. In addition, when the window size is larger than 3.5s the TP rate and TN rate are lower than 74.64% and 85.24%, respectively. The observation shows that the highest detection accuracy requires a suitably set sliding window size for training. Thus, based on the result shown in the figure, we set the sliding window size of our training dataset to 2s for best accuracy.

V. CONCLUSIONS

In this paper, we proposed a driving fatigue detection system using the received phase values in RFID tag responses. We designed the proposed NodTrack system, including data sensing, movement feature extraction, offline training, and online drowsy detection modules. Features were extracted by filtering and differentiating the phase difference between two tags, which were attached to the back side of a hat worn by the driver. We employed an LSTM autoencoder model to learn the nodding features. Nodding motion was detected by the divergence between the input signal and the reconstructed signal of the learning model. The high detection accuracy of the prosed system was demonstrated by experiments with commercial tags and readers.

ACKNOWLEDGMENT

This work is supported in part by the NSF under Grant CNS-1702957.

REFERENCES

 National Road Safety Foundation, "Drowsy driving," 2018 (accessed April 24, 2018). [Online]. Available: https://www.ghsa.org/issues/ drowsy-driving

- [2] National Highway Traffic Safety Administration, "U.S. DOT Announces 2017 Roadway Fatalities Down," 2018 (accessed April 24, 2018). [Online]. Available: https://www.nhtsa.gov/press-releases/ us-dot-announces-2017-roadway-fatalities-down
- [3] B. T. Jap, S. Lal, P. Fischer, and E. Bekiaris, "Using EEG spectral components to assess algorithms for detecting fatigue," *Elsevier Expert Systems with Applications*, vol. 36, no. 2, pp. 2352–2359, Mar. 2009.
- [4] W.-B. Horng, C.-Y. Chen, Y. Chang, and C.-H. Fan, "Driver fatigue detection based on eye tracking and dynamic template matching," in *Proc. IEEE ICNSC'04*, Taipei, Taiwan, Mar. 2004, pp. 7–12.
- [5] W. Jia and H. Peng, "Wifind: Driver fatigue detection with fine-grained Wi-Fi signal features," in *Proc. IEEE GLOBECOM 2017*, Singapore, Dec. 2017, pp. 1–6.
- [6] Y. Xie, F. Li, Y. Wu, S. Yang, and Y. Wang, "D 3-Guard: Acoustic-based drowsy driving detection using smartphones," in *Proc. IEEE INFOCOM'19*, Paris, France, Apr./May 2019, pp. 1–9.
- [7] Y. Ma, N. Selby, and F. Adib, "Drone relays for battery-free networks," in *Proc. ACM SIGCOMM'17*, Los Angeles, CA, Aug. 2017, pp. 335–347.
- [8] J. Zhang, Z. Yu, X. Wang, Y. Lyu, S. Mao, S. C. Periaswamy, J. Patton, and X. Wang, "RFHUI: An intuitive and easy-to-operate human-uav interaction system for controlling a UAV in a 3D space," in *Proc. EAI MobiQuitous* 2018, New York City, NY, Nov. 2018, pp. 69–76.
- [9] P. Asadzadeh, L. Kulik, and E. Tanin, "Gesture recognition using RFID technology," *Springer Personal and Ubiquitous Computing*, vol. 16, no. 3, pp. 225–234, Mar. 2012.
- [10] L. Yao, Q. Sheng, W. Ruan, T. Gu, X. Li, N. Falkner, and Z. Yang, "RF-care: Device-free posture recognition for elderly people using a passive RFID tag array," in *Proc. EAI MobiQuitous 2015*, Coimbra, Portugal, July 2015, pp. 120–129.
- [11] Y. Hou, Y. Wang, and Y. Zheng, "Tagbreathe: Monitor breathing with commodity RFID systems," in *Proc. IEEE ICDCS 2017*, Atlanta, GA, June 2017, pp. 404–413.
- [12] C. Yang, X. Wang, and S. Mao, "AutoTag: Recurrent vibrational autoencoder for unsupervised apnea detection with RFID tags," in *Proc. IEEE GLOBECOM* 2018, Abu Dhabi, UAE, Dec. 2018, pp. 1–7.
- [13] X. Wang, J. Zhang, Z. Yu, E. Mao, S. Periaswamy, and J. Patton, "RF Thermometer: A temperature estimation method with commercial UHF RFID tags," in *Proc. IEEE ICC'19*, Shanghai, China, May 2019, pp. 1–6
- [14] C. Yang, X. Wang, and S. Mao, "SparseTag: High-precision backscatter indoor localization with sparse RFID tag arrays," in *Proc. IEEE SECON* 2019, Boston, MA, June 2019.
- [15] I. S. R. R. A. Note, "Low level user data support," *Impinj, Seattle, Washington, USA*, 2013.
- [16] T. Wei and X. Zhang, "Gyro in the air: Tracking 3D orientation of batteryless internet-of-things," in *Proc. ACM MobiCom'16*, New York City, NY, Oct. 2016, pp. 55–68.
- [17] C. Duan et al., "Robust spinning sensing with dual-rfid-tags in noisy settings," IEEE Trans. Mobile Comput, in press.